

Arecibo and FAST Timing Follow-up of twelve Millisecond Pulsars Discovered in Commensal Radio Astronomy FAST Survey

C. C. Miao,^{1,2} * W. W. Zhu¹ †, D. Li,¹ ‡, P. C. C. Freire⁴ , J. R. Niu^{1,2} , P. Wang¹ , J. P. Yuan⁶, M. Y. Xue¹ , A. D. Cameron³ , D. J. Champion⁴ , M. Cruces⁴ , Y. T. Chen^{1,2}, M. M. Chi⁸ , X. F. Cheng⁸, S. J. Dang⁵, M. F. Ding⁸, Y. Feng⁷ , Z. Y. Gan⁹, G. Hobbs³ , M. Kramer⁴ , Z. J. Liu⁵, Y. X. Li⁹, Z. K. Luo⁹, X. L. Miao¹, L. Q. Meng^{1,2} , C. H. Niu¹ , Z. C. Pan¹ , L. Qian¹ , Z. Y. Sun⁹, N. Wang⁶, S. Q. Wang⁶, J. B. Wang⁶, Q. D. Wu⁶, Y. B. Wang⁹, C. J. Wang⁹, H. F. Wang¹⁰, S. Wang¹, X. Y. Xie⁵, M. Xie⁸, Y. F. Xiao¹¹, M. Yuan^{1,2} , Y. L. Yue¹ , J. M. Yao⁶, W. M. Yan⁶, S. P. You⁵, X. H. Yu⁵, D. Zhao⁶, R. S. Zhao⁵, L. Zhang¹ 

¹National Astronomical Observatories, Chinese Academy of Sciences, 20A Datun Road, Chaoyang District, Beijing 100101, China

²School of Astronomy and Space Science, University of Chinese Academy of Sciences, Beijing, 100049, China

³CSIRO Astronomy and Space Science, PO Box 76, Epping, NSW 1710, Australia

⁴Max-Planck Institut für Radioastronomie, Auf dem Hügel 69, D-53121 Bonn, Germany

⁵Guizhou Normal University, Guiyang 550001, China

⁶Xinjiang Astronomical Observatory, Chinese Academy of Sciences, Urumqi, Xinjiang 830011, People's Republic of China

⁷Zhejiang Lab, Hangzhou, Zhejiang 311121, People's Republic of China

⁸Fudan University, Shanghai, China

⁹Tencent Youtu Lab

¹⁰College of Computer and Information, Dezhou University, Dezhou 253023

¹¹GuiZhou University, GuiZhou 550025, China

Accepted XXX. Received YYY; in original form ZZZ

ABSTRACT

We report the phase-connected timing ephemeris, polarization pulse profiles, Faraday rotation measurements, and Rotating-Vector-Model (RVM) fitting results of twelve millisecond pulsars (MSPs) discovered with the Five-hundred-meter Aperture Spherical radio Telescope (FAST) in the Commensal radio Astronomy FAST survey (CRAFTS). The timing campaigns were carried out with FAST and Arecibo over three years. Eleven of the twelve pulsars are in neutron star - white dwarf binary systems, with orbital periods between 2.4 and 100 d. Ten of them have spin periods, companion masses, and orbital eccentricities that are consistent with the theoretical expectations for MSP - Helium white dwarf (He WD) systems. The last binary pulsar (PSR J1912–0952) has a significantly smaller spin frequency and a smaller companion mass, the latter could be caused by a low orbital inclination for the system. Its orbital period of 29 days is well within the range of orbital periods where some MSP - He WD systems have shown anomalous eccentricities, however, the eccentricity of PSR J1912–0952 is typical of what one finds for the remaining MSP - He WD systems.

Key words: surveys – pulsars: general – binaries: general

1 INTRODUCTION

Millisecond pulsars (MSP) are a special kind of neutron stars that rotate tens to hundreds of times per second and have significantly lower magnetic field strengths when compare to the normal pulsar population. Not only is their formation and evolution a topic of great interest, but as well their role as tools for experiments in fundamental physics – which is achieved through pulsar timing. Examples are: performing tests of general relativity with binary neutron star

systems (Taylor & Weisberg 1989; Manchester 2015; Kramer et al. 2021), which include tests of the strong equivalence principle (SEP, Archibald et al. 2018; Voisin et al. 2020) and specifically of the Lorentz invariance and conservation law (Shao et al. 2013; Zhu et al. 2019a; Miao et al. 2020) and to measure neutron star masses, which constrain the equation of state of matter at super-nuclear density (De-morest et al. 2010; Antoniadis et al. 2013; Fonseca et al. 2021), a fundamental unsolved problem in astrophysics and nuclear physics (Özel & Freire 2016). Furthermore, pulsar timing arrays, or PTAs (Hobbs et al. 2010) might soon detect low-frequency gravitational waves (Kramer et al. 2004).

Since their initial discovery over 54 years ago (Hewish et al. 1968),

* E-mail: miaocc@nao.ac.cn

† E-mail: zhuww@nao.cas.cn

‡ E-mail: dili@nao.cas.cn

over 3100 pulsars have been discovered and listed in Australia Telescope National Facility (ATNF) Pulsar Catalogue PSRCAT¹ (version 1.6.5) (Manchester et al. 2005). The surveys that found them (like the GBT350, Sayer et al. 1997, PMPS, Manchester et al. 2001, PALFA, Cordes et al. 2006, HTRU-S, Keith et al. 2010, GBNC, Stovall et al. 2014, AO327, Deneva et al. 2013, HTRU-N, Barr et al. 2013 and LOTAAS, Sanidas et al. 2019) are driven by the need to discover all sorts of new systems: more relativistic binaries for gravity experiments, MSPs with better timing precision for PTAs, neutron stars with larger masses for probing the EOS, and the discovery of unusual systems, like the pulsar in a triple system which proved to be a superb laboratory for precise tests of the SEP. With their much higher spectral and time resolution, the more recent surveys are discovering a much larger fraction of MSPs relative to previous surveys (e.g., Parent et al. 2019; Martinez et al. 2019), including pulsars in highly relativistic systems (Stovall et al. 2018; Cameron et al. 2018), at least compared to any previous systems containing radio pulsars.

The Five-hundred-meter Aperture Spherical radio Telescope (FAST) (Nan 2008; Nan et al. 2011) is currently the largest single-dish radio telescope. Early FAST commissioning observations are ongoing since August 2017 with the ultra-wideband receiver (UWB, 270-1650 MHz, Tsys 65 K) in drift scan observing mode, helping to gauge the feasibility of the drift-mode pulsar search program. The low-frequency system on FAST was decommissioned in May of 2018. We then started to implement the pilot Commensal Radio Astronomy FAST Survey (Li et al. 2018, CRAFTS²) scans with the FAST 19-beam L-band (1050-1450 MHz) receiver. After January 2020, FAST finished its commissioning operation and started its science operation (Jiang et al. 2020). In January 2020, the newly formed FAST Science Committee approved five major surveys, all of which used the L-band 19beam feed-horn array. The ongoing surveys, such as the CRAFTS and the FAST Galactic Plane Pulsar Snapshot Survey (Han et al. 2021, GPPS) are expected to discover many more MSPs, and thus make a significant contribution to the PTA experiments. Until December 2021, combining all pulsars discovered in the CRAFTS and the early FAST commission survey, more than 160 new pulsars³ (include 35 MSPs) (Qian et al. 2019; Zhang et al. 2019; Cameron et al. 2020; Wang et al. 2021a; Cruces et al. 2021; Wang et al. 2021c), 4 FRBs (Zhu et al. 2020; Niu et al. 2021) and 1 radio-faint MSP from the Fermi-LAT unassociated source (Wang et al. 2021b; You et al. 2021) have been discovered in total ~ 850 hours. The area searched represents 15% of the sky that FAST can see.

The CRAFTS search mode observations are conducted in the drift-scan mode where the telescope is held fixed at the meridian while the sky drifts past the telescope beams. This increases the position uncertainty of the newly discovered pulsars (see Cruces et al. 2021 for more details). With the rapid growth of pulsar candidates, we strive to swiftly follow up FAST discoveries through international collaborations. Our team members from Parkes, Effelsberg, and Green Bank radio Telescopes are working on the CRAFTS pulsar follow-up (Cameron et al. 2020; Cruces et al. 2021; Wang et al. 2021a). Cameron et al. 2020 reported confirmation and timing results of 11 isolated pulsars found in CRAFTS with the 64-m Parkes Radio Telescope. Cruces et al. 2021 presented confirmation and timing results of 10 CRAFTS pulsars, including 9 isolated pulsars and 1 neutron star - Carbon-Oxygen white dwarf (WD) binary system, with the 100-m Effelsberg radio-telescope. Wang et al. 2021a showed con-

Table 1. The timing observation parameters include the central frequency, bandwidth, number of channels, and sampling time.

Telescope	f_{center} (MHz)	Bandwidth (MHz)	n_{chan}	T_{samp} μs
FAST	1250 MHz	500 MHz	4096	49.152
	1250 MHz	500 MHz	1024	49.152
Arecibo	1290 MHz	800 MHz	2048	64

firmation results and nulling studies of 7 CRAFTS pulsars with the Arecibo 305-m Telescope.

In this work, we report on the timing results of twelve MSPs discovered in FAST’s CRAFTS survey with FAST and also with the Arecibo 305-m radio telescope (Arecibo). In section 2, we describe our observation settings and epochs. The data analyses are shown in section 3. Polarization pulse profiles, timing residuals, phase-connected timing solutions, and Rotating-Vector-Model (RVM) fitting results are presented in section 4. We discuss the distribution of orbital period and eccentricity in MSP-WD systems and summarized our findings in section 5.

2 OBSERVATIONS

The parameters of the FAST and Arecibo observations setup are listed in the Tab. 1. Observations taken at Arecibo were taken with the Arecibo L-wide receiver and Puerto Rico Ultimate Pulsar Processing Instrument (PUPPI) backend. The frequency range of the Arecibo L-wide receiver was 980 MHz - 1780 MHz. Due to the RFI and low response at the edges of the band, the effective band of this receiver was from 1150 MHz to 1750 MHz. Observations at FAST are taken with the central beam of the FAST 19-beam receiver (Jiang et al. 2020). Its frequency coverage is 1000 MHz - 1500 MHz and the effective band is from 1050 MHz to 1450 MHz. Observations at FAST were taken by two different projects and the receiver configurations used were different (as shown in Tab. 1). Observation data are all recorded in pulsar search mode with full-Stokes. Each pulsar observation starts with a one-minute calibration noise diode for the polarization calibration, while the flux calibrator observations are not performed. The integration time for each session of Arecibo is 1200 seconds and that of FAST is 300 seconds.

The confirmation observations of these pulsars were made by the FAST and the regular follow-up timing observations were made by both FAST and Arecibo. In the first two weeks, we performed observations on days 1, 2, 3, 5, 10, and 15. After these, we performed observations every 30~60 days.

Six MSPs are in Arecibo’s declination range; we followed them up with Arecibo from MJD 58883 to MJD 59055. The other six are followed up with FAST. After the collapse of Arecibo, all of the remaining timing campaigns were continued using FAST. The FAST observations were taken from MJD 58620 to MJD 59530. Epochs of observations reported in this work are shown in Fig. 1. The color of the markers represents observations at the different telescopes and each marker represents each observation session.

3 DATA ANALYSIS

Unlike other new pulsar follow-up programs, where an initial ephemeris is derived for subsequent data to taken in timing and fold

¹ <https://www.atnf.csiro.au/research/pulsar/psrcat/>

² <https://crafts.bao.ac.cn>

³ The list of confirmed pulsars <https://crafts.bao.ac.cn/pulsar>

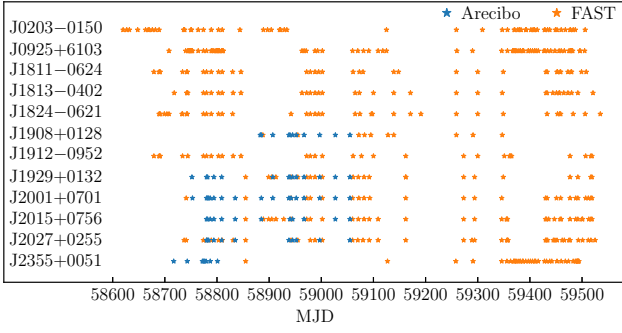


Figure 1. Observation epochs of 12 MSPs. The color of markers represents observation taken with different telescopes. Blue markers are Arecibo observations and orange markers are FAST observations.

mode. We take all our observation data in the incoherent searching mode. But we still need to derive an ephemeris to fold the data and derive TOAs.

To derive an initial ephemeris, we fold the raw data with an observed spin period (P_{obs}) and dispersion measure (DM) without an ephemeris. To determine these two parameters (P_{obs} , DM), we processed the first several observations with a pulsar search and analysis software, PRESTO⁴ (V3.0.1) (Ransom 2011). With tools from PRESTO, the raw data were cleaned off the radio frequency interference (RFI) and folded with an optimal P_{obs} and DM. Since the initial observations are often short (5–10 min long), we could not constrain the \dot{P}_{obs} of the pulsar from a single observation. From the first few months’ follow-up observations results, we confirmed that only one pulsar is isolated and the other pulsars are in binary systems.

For the isolated pulsar, the initial ephemeris file contains the coordinates of the pulsar, the estimated spin frequency ($F0 = 1/P0$), a fiducial spin frequency derivative (F1) of 0 (to be constrained after several observations), and the measured DM at a given MJD epoch. This is often enough for fitting observations within several months and updates are needed when observations span longer than half a year. We fold the data using DSPSR⁵ (van Straten & Bailes 2011). The folded data were cleaned of RFI and down-sampled in frequency with tools from PSRCHIVE⁶ (Hotan et al. 2004). The times of arrival (TOAs) are created by using pat⁶.

For the pulsars in binary systems, the initial ephemeris file contains coordinates, estimated F0, estimated F1, DM, and the Keplerian parameters describing the orbital motion. Some of these parameters cannot be well constrained with few beginning observations, but have to be solved by using phase-connected TOAs from a long time span.

We use several initial observations to estimate the Keplerian binary parameters orbital period (P_b), the epoch of periastron passage (T_0), and projected semi-major axis (x) using `fit_circular_orbit.py`⁴. The input is the optimal F0 values from folding each observation with the `prepfold` command. `fit_circular_orbit.py` gives the estimation of P_b , T_0 and x while assuming that the orbital eccentricity (e) is zero.

The above initial estimated circular orbit parameters are often good enough to fold the first several observations from which they were derived. We employ the ELL1 (Lange et al. 2001; Zhu et al. 2019a) timing model in TEMPO⁷ (Nice et al. 2015) to describe the orbit and

fold the data using DSPSR. The folded data were processed as same as the isolated pulsar. The times of arrival (TOAs) are derived by using pat.

After we apply our initial ephemeris to fold and derive TOAs, and then iteratively improve this ephemeris with the TOAs, it quickly converges to a well-constrained ephemeris that includes only spin frequency F0 and fitted circular orbital parameters. This new iteratively-fitted circular-orbit ephemeris is already good enough for folding most of the subsequent observations, but not good enough to phase connect them.

To find the phase-connected timing solution to all the TOAs, we use the TEMPO (Nice et al. 2015) and TEMPO2⁸ (Hobbs et al. 2006) softwares. In the final phase coherent timing solutions, we fit the pulsar’s astrometry coordinates, intrinsic F0, F1, DMc and five Keplerian orbital parameters (P_b , T_{asc} , x , ϵ_1 , ϵ_2) and only fit the pulsar’s astrometry coordinates, intrinsic F0, F1, DM for the isolated pulsar. The integration time of each TOA is one minute for both FAST and Arecibo. We reduce the data from high signal-to-noise ratio (S/N) observations by summing their bands into 2 sub-bands and the other observations are summed into 1 sub-band. Some of our binary solutions are found with the help of DRACULA⁹ (Freire & Ridolfi 2018).

All of our final phase-connected timing solutions for binary systems are described by using the ELL1 model. This model was developed for small-eccentricity binaries and replaced T_0 , ω and e by the time of ascending node (T_{asc}) and the Laplace–Lagrange parameters ($\epsilon_1 \equiv e \sin \omega$, $\epsilon_2 \equiv e \cos \omega$). The usage of T_{asc} , ϵ_1 and ϵ_2 breaks the high correlation between T_0 and ω in binary systems with small eccentricities and makes it a good model to connect TOAs for near-circular orbits. For many of these nearly-circular binaries, the ELL1 model can provide a decent description of the timing data because of the recent inclusion of $x e^2$ order terms in the description of the geometric delays in the orbit (Zhu et al. 2019a).

To derive the polarization profile for the pulsars, we conducted noise injection for polarimetric calibration at the beginning of each observation. After the polarimetric calibration, the highest S/N observation of each pulsar is selected and used to search the Faraday rotation measure (RM) with RM-TOOLS¹⁰ (Purcell et al. 2020). The RM of ionosphere RM_{iono} are computed using `ionFR`¹¹ (Sotomayor-Beltran et al. 2013). We also fitted the Rotating Vector Model (Radhakrishnan & Cooke 1969; Everett & Weisberg 2001, RVM) to model the viewing geometry of these with `psrmodel` from PSRCHIVE⁶. We present the best-fit RVM result when a reasonable fit can be achieved, alongside the polarimetry measurements in fig. 3.

4 RESULTS

Timing residuals of 2.5 years are shown in Fig. 2. To ensure the TOA residuals χ^2 are ~ 1 , we weighted the TOA uncertainties by using EFAC¹². The TOAs created from FAST observations are shown in blue and TOAs created from Arecibo observations are shown in red.

The profiles shown in Fig. 3 are from the observation of the highest S/N. We derive the observed RMs from these profiles and list the interstellar RMs in Tab. 2 after removing the RM_{iono} . We present the RM-corrected polarization profiles at 1.25 GHz in Fig. 3. We also display the linear polarization position angle (PA) of these MSPs

⁴ <https://github.com/scotttransom/presto>

⁵ <http://dspsr.sourceforge.net>

⁶ <http://psrchive.sourceforge.net>

⁷ <http://tempo.sourceforge.net>

⁸ <https://bitbucket.org/psrsoft/tempo2>

⁹ <https://github.com/pfreire163/Dracula>

¹⁰ <https://github.com/CIRADA-Tools/RM-Tools>

¹¹ <https://github.com/csobey/ionFR>

¹² a scaling factor applied to TOA uncertainties

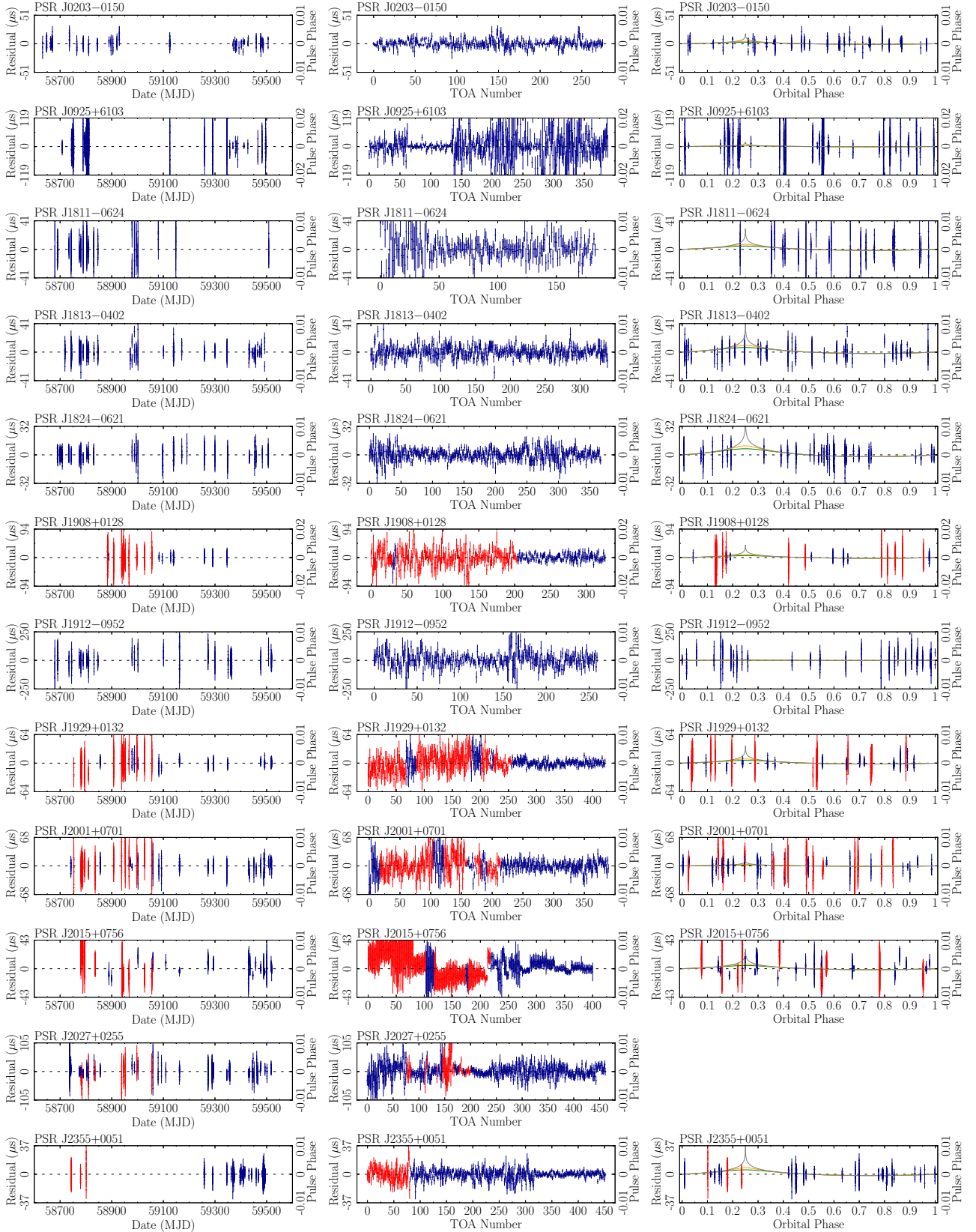


Figure 2. The best post-fit timing residuals of the twelve millisecond pulsars obtained using the timing solutions in Tables 3–5. The 3 columns are respectively MJD v.s. residual plots, TOA-number v.s. residual plots and orbital phase v.s. residual plots. The orbital phase v.s. residual plot of the only isolated pulsar J2027+0255 is not shown. The grey, orange, and green solid line shows the Shapiro delay functional form assuming the orbital inclination angle $i = 60^\circ, 75^\circ, 90^\circ$. The blue and red data points represent observations with FAST and Arecibo respectively.

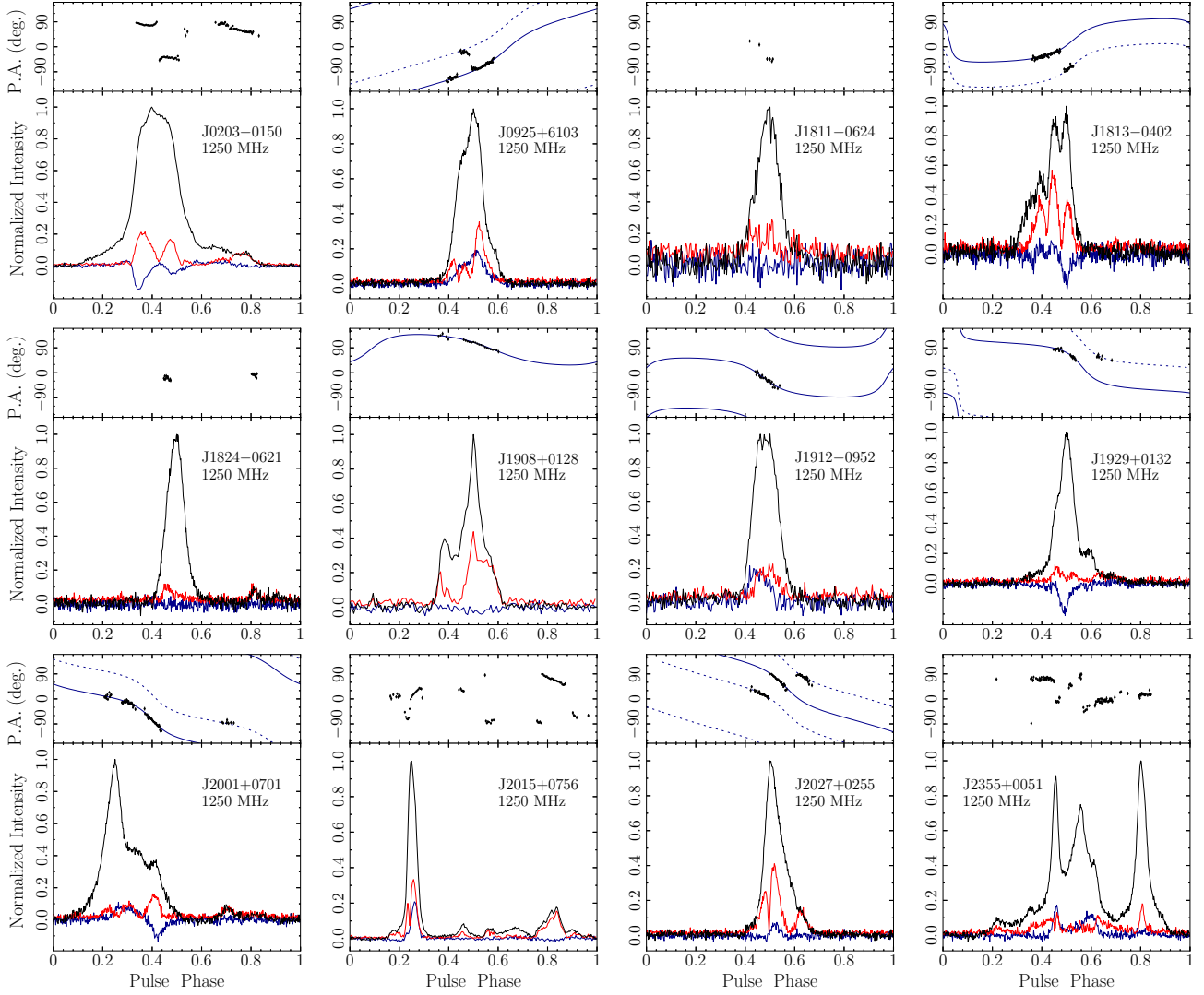


Figure 3. Integrated polarization profiles of 12 recycled MSPs (J0203–0150, J0925+6103, J1811–0624, J1813–0402, J1824–0621, J1908+0128, J1912–0952, J1929+0132, J2001+0701, J2015+0756, J2027+0255, J2355+0051) at 1.25 GHz. Top panel of each subplot: The plot of linear polarization position angle (PA) and RVM best-fit result. The black dots with error bars are the original PA points. The blue solid line represents the best-fit RVM model and the blue dashed line is 90° shifted from the RVM model to indicate potential orthogonal mode. We present the RVM fitting results of 7 pulsars here. The potential orthogonal mode emission is not taken into account when fitting for the RVM model. Bottom panel of each subplot: The plot of normalized pulsar polarization profile. The total intensity (I), linear polarization (L), and circular polarization (V) profiles are represented by black, red, and blue solid lines, respectively.

and Rotating-Vector-Model (Radhakrishnan & Cooke 1969, RVM) fitting results in Fig. 3. As described in (Everett & Weisberg 2001), the linear polarization PA is a function of the magnetic inclination angle (α), the angle between the line of sight and the rotation axis (ζ), the reference position angle (ψ_0), and longitude of the fiducial plane (ϕ_0). Seven MSPs in this paper with well-defined PA are successfully modeled using the RVM model and the best-fit results are listed in Tables 3 to 5.

Fig. 4 corresponds to a $P-\dot{P}$ diagram of 33 new pulsars discovered in CRAFTS with proper timing solutions and known pulsars listed in the PSRCAT (version 1.6.5). These newly 33 pulsars consist of 11 pulsars reported in (Cameron et al. 2020), 10 pulsars reported in (Cruces et al. 2021), and 12 pulsars reported in this work. The $P-\dot{P}$ distribution of MSPs reported in this work well coincide with the distribution of known MSPs.

The timing ephemeris of these 12 MSPs are reported in Tables 3 to 5. These timing solution are obtained using JPL DE438¹³ solar system ephemeris. The latest FAST site position can be found in Qian & Yue 2020 and is already updated in the latest version of TEMPO (Version 13.103). In our analysis, we have accounted for the FAST-site to GPS clock difference.

The minimum companion mass $m_{c,\min}$ and median companion mass $m_{c,\text{med}}$ listed in the Tabs. 3, 4 and 5 are calculated separately assuming the orbital inclination of $i = 90^\circ, 60^\circ$ and a pulsar mass of $1.4 M_\odot$. We calculate the DM distances (d) by using YMW 16 (Yao et al. 2017) models for the galactic distribution of free electrons. We estimate the spin-down luminosity (\dot{E}), the surface magnetic

¹³ <ftp://ssd.jpl.nasa.gov/pub/eph/planets/bsp/de438.bsp>

Table 2. Faraday rotation measurement of the 12 MSPs. These measurements are made from the highest S/N follow-up observation of each pulsar. We list the measured RM (RM_{meas}) and Faraday rotation from ionospheric (RM_{iono}). The RM_{iono} are computed using ionFR (Sotomayor-Beltran et al. 2013).

Pulsar name	Observation epoch (MJD)	RM_{meas} (rad m ⁻²)	RM_{iono} (rad m ⁻²)	RM_{PSR} (rad m ⁻²)
J0203–0150	58844.5245	3.9(7)	1.3(1)	2.6(8)
J0925+6103	58749.0424	−18.1(1)	0.18(3)	−18.28(13)
J1811–0624	58789.3688	22(1)	1.9(1)	20.1(11)
J1813–0402	58789.3826	24(1)	1.9(1)	22.1(11)
J1824–0621	59506.3680	84.6(4)	3.6(2)	81.0(6)
J1908+0128	59259.0495	−34.7(2)	0.9(1)	−35.6(3)
J1912–0952	58774.4385	−72.2(3)	3.2(2)	−75.4(5)
J1929+0132	59348.9229	−69(2)	2.4(1)	−71.4(21)
J2001+0701	59273.1063	−107.6(4)	1.1(1)	−108.7(5)
J2015+0756	59355.9070	−70.7(6)	1.6(1)	−72.3(7)
J2027+0255	58774.4528	−113.0(1)	2.7(1)	−115.7(2)
J2355+0051	59490.6882	4.3(6)	4.4(2)	−0.1(8)

field (B_{surf}) and the characteristic age τ_c from intrinsic period (P) and intrinsic spin period derivative (\dot{P}) according to the equations presented in Lorimer & Kramer 2012.

Our mean flux density measurements are reported in the Tabs. 3, 4 and 5. For the observations taken with FAST, we estimate the pulsar flux density at 1250 MHz by using the radiometer equation (Lorimer & Kramer 2012).

$$S_{\text{mean}} = \frac{(S/N)\beta T_{\text{sys}}}{G\sqrt{n_p t_{\text{obs}} \Delta f}} \sqrt{\frac{W}{P - W}} \quad (1)$$

The gain (G) and system temperature (T_{sys} , K) of the FAST telescope are the functions of the observation zenith angle (θ_{ZA}) and following the formulas described in Jiang et al. 2020. Our observations are conducted with the 2 polarizations, an effective bandwidth (Δf) of 400 MHz and a correction factor β of 1. The equivalent width W (s), S/N are estimated from the summed pulse profile.

PSR J0203–0150 is an MSP with a spin period of 5.17 ms and was first reported in Yu et al. (2020). It is in a 49.96 day binary orbit with an eccentricity of 0.0001938. As shown in Fig. 3, this MSP has an extremely wide single-component pulse profile. The W_{10} pulse width (corresponding to about 10 percent of the maximum intensity) of PSR J0203–0150 is 2.54 ms and the duty cycle of on pulse area is more than 70 %. The complex PA swing of the pulsar did not yield a satisfactory RVM model fit.

PSR J0925+6103 is a 5.98 ms pulsar with a DM of 21.6 cm⁻³ pc. It is in a 2.45 day binary orbit with an eccentricity of 0.7×10^{-5} . We had observed this pulsar 78 times and it only showed up with enough S/N in 33 observation sessions. Within those observations with high S/N, we found no flux density variations in short time scale. The scintillation timescale for pulsars in binary systems may vary with the change of orbital phase due to modulation of the orbital velocity; however, we found that detections happen at random orbital phases, further proving that the interstellar scintillation timescale is larger than the observation length. In this case, we think the non-detections are likely caused by the strong slow-varying interstellar scintillation or the intrinsic variation of pulsar flux density.

PSR J1811–0624 is a 4.14 ms pulsar at the DM of 158.8 cm⁻³ pc with a low polarized, single component pulse profile. It is in a 9.38 day binary orbit with an eccentricity of 2.64×10^{-5} . This MSP

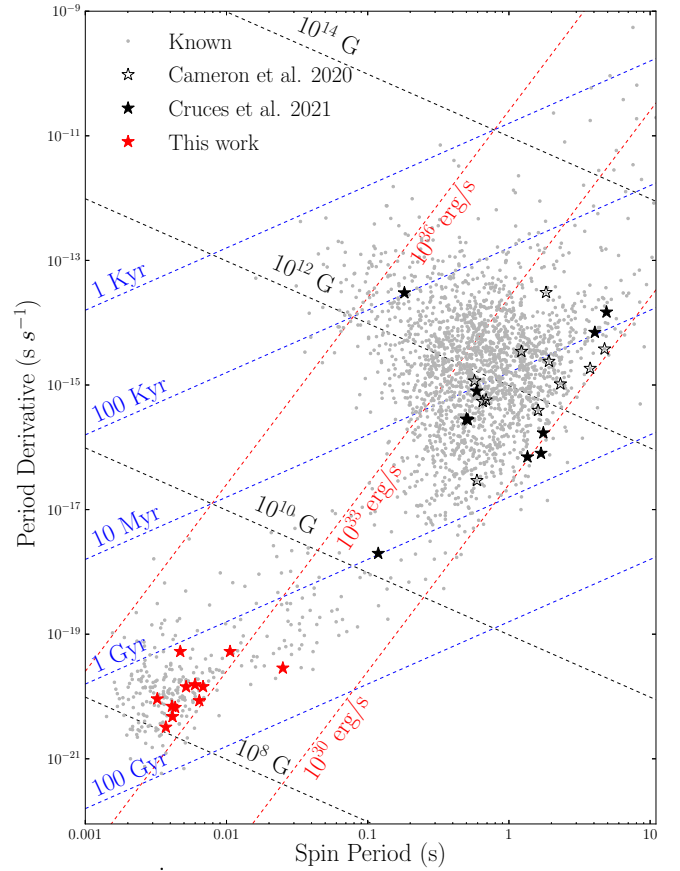


Figure 4. A P - \dot{P} diagram of known pulsars and new pulsars presented in this work. The grey dots are 2438 pulsars listed in the PSRCAT (version 1.6.5) with well-measured P and \dot{P} . The star symbols are pulsars discovered in CRAFTS with well-measured parameters. The open-black stars represent pulsars reported in (Cameron et al. 2020) and filled-black stars represent pulsars reported in (Cruces et al. 2021). The filled-red stars represent MSPs reported in this work. Lines of characteristic age (blue-dotted), surface magnetic field strength (black-dotted), and spin-down luminosity (red-dotted) are also shown in this plot.

displays a low S/N in all of our observations. The few measurable PA points make the RVM model fitting impossible.

PSR J1813–0402 has a spin period of 4.107 ms, a DM of 71.3 cm⁻³ pc and an estimated DM distance of 2.23 kpc. It is in a 10.56 day binary orbit with an eccentricity of 0.416×10^{-5} .

PSR J1824–0621 is a 3.23 ms pulsar with the DM of 131.0 cm⁻³ pc. It is in a 100.9 day binary orbit with an eccentricity of 0.00022931. This system has the longest orbit period from our data set. We only measured few PA points in small ranges of its spin phase and could not get an acceptable RVM model out of them.

PSR J1908+0128 is a 4.702 ms pulsar with the DM of 75.05 cm⁻³ pc, implying a DM distance to 2.63 kpc (YWM16 model Yao et al. 2017). As the part of a wide binary system, the orbital period of this MSP is 84.192 day and the eccentricity is 0.0002654.

PSR J1912–0952 has a spin period of 25.068 ms and a DM of 126.3 cm⁻³ pc. This pulsar is in an interesting binary system with a orbital period of 29.5 days and an eccentricity of 4.9×10^{-5} (discussed in the Section 5).

PSR J1929+0132 is a 6.418 ms pulsar with the DM of 53.45 cm⁻³ pc. It is in a 9.26 day binary orbit with an eccentricity of 0.848×10^{-5} . Its profile has a single component with a Gaussian-like comparative weak tail.

Table 3. Best-fit TEMPO timing parameters for pulsar J0203–0150, J0925+6103, J1811–0624, J1813-0402.

Pulsar name	J0203–0150	J0925+6103	J1811–0624	J1813–0402
<i>Measured Parameters</i>				
Data span (MJD)	58632 - 59506	58708 - 59497	58679 - 59509	58718 - 59493
Number of TOAs	276	389	184	340
Fit χ^2 /number of degrees of freedom	264.00/264	377.18/377	172.07/172	328.01/328
Post-fit RMS of residuals (μ s)	4.843	12.530	12.478	6.888
EFAC	1.22	1.14	1.12	1.06
Right Ascension, α (J2000)	02:03:33.91215(4)	09:25:17.5451(2)	18:11:18.0861(2)	18:13:34.93602(2)
Declination, δ (J2000)	−01:50:01.5874(9)	61:03:04.104(4)	−06:24:37.42(3)	−04:02:47.8226(12)
Spin Frequency, ν (s^{-1})	193.299397611600(14)	167.15383952386(15)	241.2147450264(12)	243.51284588890(2)
Spin frequency derivative, $\dot{\nu}$ (s^{-2})	$-5.336(4) \times 10^{-16}$	$-4.51(4) \times 10^{-16}$	$-2.8(2) \times 10^{-16}$	$-4.117(7) \times 10^{-16}$
Dispersion Measure, DM (cm^{-3} pc)	19.2188(7)	21.6442(11)	158.826(3)	71.3474(9)
Flux density at 1.25 GHz (μ Jy)	270(33)	195(59)	102(10)	148(12)
Binary model	ELL1	ELL1	ELL1	ELL1
Orbital Period, P_b (day)	49.96398986(5)	2.452162593(3)	9.38782916(5)	10.560352898(4)
Projected semi-major axis, x (lt-s)	12.5803188(4)	1.759392(3)	6.561124(2)	9.4263516(5)
Epoch of the ascending node, Tasc (MJD)	59395.8714674(6)	58688.7741838(6)	58692.1778781(8)	58716.88174915(15)
$e \sin \omega$, ϵ_1 (10^{-5})	−19.375(8)	−0.5(2)	−0.38(5)	−0.291(17)
$e \cos \omega$, ϵ_2 (10^{-5})	0.296(8)	0.4(3)	2.61(12)	−0.297(12)
<i>Fixed Parameters</i>				
Solar System Ephemeris	DE438	DE438	DE438	DE438
Reference epoch for α , δ , and ν (MJD)	59505.767371	59505.003027	58743.432922	58718.546229
<i>Derived Parameters</i>				
Galactic longitude, l ($^\circ$)	160.317	153.506	22.604	24.971
Galactic latitude, b ($^\circ$)	−59.365	41.833	5.923	6.534
DM-derived distance (YMW16 model), d (kpc)	1.84	1.98	5.8	2.23
Spin-down luminosity, \dot{E} (10^{33} erg s^{-1})	4.074(3)	2.97(3)	2.6(2)	3.960(7)
Surface magnetic field, B_{surf} (10^8 G)	2.7505(11)	3.143(16)	1.42(5)	1.7087(15)
Characteristic age, τ_c (Gyr)	5.724(4)	5.86(6)	13.8(11)	9.345(17)
Inferred eccentricity, e (10^{-5})	19.377(8)	0.7(2)	2.64(12)	0.416(15)
Mass function, f (10^{-3}) M_\odot	0.85628165(9)	0.972401(5)	3.440807(4)	8.0636184(14)
Minimum companion mass, $m_{c,min}$ (M_\odot)	0.125	0.131	0.207	0.283
Median companion mass, $m_{c,med}$ (M_\odot)	0.146	0.153	0.242	0.334
Longitude of the fiducial plane, ϕ_0 ($^\circ$)	−	241(4)	−	131(1)
Reference position angle ψ_0 ($^\circ$)	−	50(5)	−	−56(3)
Magnetic inclination angle, α ($^\circ$)	−	41(15)	−	74(1)
Viewing angle, ζ ($^\circ$)	−	23(10)	−	79(2)

PSR J2001+0701 has a spin period of 6.82 ms and a DM of $63.3 \text{ cm}^{-3} \text{ pc}$. It is in a 5.22 day binary orbit with an eccentricity of 2.25×10^{-5} . The profile contains a broad main pulse component and a little, divided, and nearly 100 percent linear polarized component. There is an orthogonal mode jumps between the PA swing of these two components.

PSR J2015+0756 is the pulsar with a spin period of 4.32 ms and a DM of $36.4 \text{ cm}^{-3} \text{ pc}$. It is in a 6.45 day binary orbit with an eccentricity of 0.308×10^{-5} . This MSP has the most complex pulse profile in our data set. The profile is composed of one narrow main pulse and five broad components. These components are all linked by the bridge of intermediate emission. The linear and circular polarization of the main pulse is normal. The second, third, and fifth components are highly linearly polarized, while the other following components have a low level of linear and circular polarization.

PSR J2027+0255 is the only isolated pulsar in our paper with a spin period of 10.596 ms and a DM of $51.1 \text{ cm}^{-3} \text{ pc}$. Its profile is a broad, single component pulse. The linear polarization consists of three components and there are two orthogonal mode jumps in the PA swing.

PSR J2355+0051 is a 3.719 ms pulsar at the DM of $11.14 \text{ cm}^{-3} \text{ pc}$. It is in a 11.75 day binary orbit with an eccentricity of 0.135×10^{-5} . The estimated DM distance is 0.9548 kpc the closest and the nearest pulsar in our source list. PSR J2355+0051 is detected only 24 times out of 66 observation sessions. The strong interstellar scintillation or variation of pulsar flux density is likely the reason for these non-detections (the same reasons as PSR J0925+6103). The unusually wide profile consists of three main pulse components and some smaller structures alongside them. We failed to get a credible RVM fit for the complex PA swing.

5 DISCUSSION AND CONCLUSION

The binaries in our sample have companion masses that are consistent with the prediction of [Tauris & Savonije \(1999\)](#) for MSPs with Helium white dwarf (He WD) systems (see Fig. 5, bottom panel); their spin periods are also well within the typical range observed for such systems. This suggests that these systems are also MSP - He WD systems. We searched the potential counterparts at the Gaia DR2 ([Gaia](#)

Table 4. Best-fit TEMPO timing parameters for pulsar J1824–0621, J1908+0128, J1912–0952, J1929+0132.

Pulsar name	J1824–0621	J1908+0128	J1912–0952	J1929+0132
<i>Measured Parameters</i>				
Data span (MJD).....	58689 - 59507	58883 - 5934	58679 - 59520	58753 - 59520
Number of TOAs.....	368	328	260	424
Fit χ^2 /number of degrees of freedom.....	356.05/356	315.01/315	248.00/248	411.12/411
Post-fit RMS of residuals (μ s).....	4.960	13.187	47.834	8.918
EFAC.....	1.0	1.11	1.2	1.34
Right Ascension, α (J2000).....	18:24:15.81954(2)	19:08:18.80366(12)	19:12:12.2482(3)	19:29:42.52833(2)
Declination, δ (J2000).....	–06:21:56.7918(13)	01:28:22.714(2)	–09:52:51.748(16)	01:32:46.5630(13)
Spin Frequency, ν (s^{-1}).....	309.30868547671(2)	212.66079094525(7)	39.89141833615(4)	155.80651370922(2)
Spin frequency derivative, $\dot{\nu}$ (s^{-2}).....	$-8.749(9) \times 10^{-16}$	$-2.383(5) \times 10^{-15}$	$-4.55(13) \times 10^{-17}$	$-2.078(6) \times 10^{-16}$
Dispersion Measure, DM (cm^{-3} pc).....	131.0313(18)	75.0575(17)	126.348(15)	53.4573(7)
Flux density at 1.25 GHz (μ Jy).....	114(6)	143(9)	195(17)	207(20)
Binary model.....	ELL1	ELL1	ELL1	ELL1
Orbital Period, P_b (day).....	100.91365361(6)	84.1922026(4)	29.4925321(5)	9.265037044(4)
Projected semi-major axis, x (lt-s).....	44.1039113(7)	38.482388(5)	5.379447(7)	8.2675144(6)
Epoch of the ascending node, Tasc (MJD).....	58734.96987117(18)	58872.1228292(12)	58685.963815(4)	58757.4798650(2)
$e \sin \omega$, ϵ_1 (10^{-5}).....	–22.809(2)	7.999(17)	–1.62(18)	–0.812(18)
$e \cos \omega$, ϵ_2 (10^{-5}).....	–2.363(2)	25.30(2)	4.6(3)	–0.244(18)
<i>Fixed Parameters</i>				
Solar System Ephemeris.....	DE438	DE438	DE438	DE438
Reference epoch for α , δ , and ν (MJD).....	58780.395162	59055.147315	58679.659247	58809.832979
<i>Derived Parameters</i>				
Galactic longitude, l ($^\circ$).....	24.16	36.17	26.415	38.712
Galactic latitude, b ($^\circ$).....	3.1	–3.08	–9.067	–7.792
DM-derived distance (YMW16 model), d (kpc).....	3.53	2.63	9.45	1.85
Spin-down luminosity, \dot{E} (10^{33} erg s^{-1}).....	10.689(11)	20.02(4)	0.072(2)	1.279(4)
Surface magnetic field, B_{surf} (10^8 G).....	1.7400(9)	5.038(5)	8.57(12)	2.372(3)
Characteristic age, τ_c (Gyr).....	5.586(6)	1.410(3)	13.9(4)	11.85(3)
Inferred eccentricity, e (10^{-5}).....	22.931(2)	26.54(2)	4.9(3)	0.848(18)
Mass function, $f(10^{-3})M_\odot$	9.0445587(4)	8.631737(3)	0.1921519(7)	7.0678361(16)
Minimum companion mass, $m_{c,\text{min}}$ (M_\odot).....	0.296	0.291	0.074	0.270
Median companion mass, $m_{c,\text{med}}$ (M_\odot).....	0.349	0.343	0.086	0.317
Longitude of the fiducial plane, ϕ_0 ($^\circ$).....	–	252(27)	203(8)	311(2)
Reference position angle ψ_0 ($^\circ$).....	–	17(27)	41(14)	69(3)
Magnetic inclination angle, α ($^\circ$).....	–	52(22)	111(7)	81(7)
Viewing angle, ζ ($^\circ$).....	–	105(30)	98(6)	101(9)

Collaboration et al. 2018)¹⁴ catalogs and none were found within a 1 arcsec radius. The distribution of orbital eccentricities (e) with P_b (see Fig. 5, top panel) also supports this case. MSP - He WD systems in globular clusters (GCs) are excluded in our sample because their eccentricities can be greatly amplified by close encounters with other stars in those systems (for a review, see Phinney 1992).

The predictions of Phinney 1992 for MSP - He WD systems are plotted in the top panel of Fig. 5 with a dashed black line. The predictions of Tauris & Savonije 1999 for MSP - He WD systems are shown in the bottom panel of Fig. 5 with the dashed black lines. The ‘orbit period gap’ (Tauris 1996) ranging from 20 to 35 days is marked by the vertical shaded bar.

This gap is interesting for several reasons: It was originally noticed because, for a long time, no systems were known to have orbital periods within that range. Now several MSP-WD systems have been found within this gap (which has now been closed), but many are somewhat anomalous; they are known as eccentric MSP binaries

(eMSPs): PSRs J0955–6150 (Camilo et al. 2015; Serylak et al. 2022), J1946+3417, (Barr et al. 2013, 2017), J1950+2414 (Knispel et al. 2015; Zhu et al. 2019b), J1618–3921 (Octau et al. 2018), and J2234+0611 (Deneva et al. 2013; Antoniadis et al. 2016; Stovall et al. 2019)); these systems are marked in Fig. 5 by the blue symbols. Although their companion masses are close to the Tauris & Savonije 1999 prediction for MSP - He WD systems, their orbital eccentricities are far from the prediction of Phinney (1992). Their formation is still mysterious (Tauris 1996; Freire & Tauris 2014; Hui et al. 2018; Han & Li 2021; Lorimer et al. 2021).

In this gap, there are also some MSP - He WD systems that do follow the prediction of Phinney (1992): PSRs J0732+2314 (Martinez et al. 2019), J1421–4409 (Spiewak et al. 2020), J1709+2313 (Lewandowski et al. 2004) and J2010+3051 (Parent et al. 2019), these are indicated in these figures by the green symbols. Their existence shows that the process that generated the eccentricities of the eMSP systems does not do so for all MSP - He WD binaries.

Here, we present another low-eccentricity binary system in this gap. PSR J1912–0952 is an MSP with an orbital period of 29.49 days and an eccentricity of 4.9×10^{-5} , which agrees with the relationship

¹⁴ <https://gea.esac.esa.int/archive/>

Table 5. Best-fit TEMPO timing parameters for pulsar J2001+0701, J2015+0756, J2027+0255, J2355+0051.

Pulsar name	J2001+0701	J2015+0756	J2027+0255	J2355+0051
<i>Measured Parameters</i>				
Data span (MJD)	58741 - 59520	58780 - 59520	58737 - 59518	58743 - 59495
Number of TOAs	391	402	463	453
Fit χ^2 /number of degrees of freedom	378.00/378	389.08/	455.09/455	440.00/440
Post-fit RMS of residuals (μ s)	11.444	6.786	16.097	3.872
EFAC	1.26	4.79	1.07	1.07
Right Ascension, α (J2000)	20:01:50.95896(3)	20:15:59.59547(5)	20:27:30.86790(7)	23:55:51.2885(14)
Declination, δ (J2000)	07:01:39.6450(13)	07:56:36.0514(16)	02:55:37.982(3)	00:51:09.57(4)
Spin Frequency, ν (s^{-1})	146.628456916751(17)	231.05446090789(9)	94.37951293046(4)	268.89004281934(9)
Spin frequency derivative, $\dot{\nu}$ (s^{-2})	$-3.092(15) \times 10^{-16}$	$-3.56(2) \times 10^{-16}$	$-4.694(19) \times 10^{-16}$	$-2.33(3) \times 10^{-16}$
Dispersion Measure, DM (cm^{-3} pc)	63.3146(13)	36.436(7)	51.132(2)	11.1452(17)
Flux density at 1.25 GHz (μ Jy)	231(18)	205(14)	186(17)	156(14)
Binary model	ELL1	ELL1	–	ELL1
Orbital Period, P_b (day)	5.22708263(2)	6.4567191424(17)	–	11.751022094(16)
Projected semi-major axis, x (lt-s)	2.2302800(15)	5.1642574(2)	–	8.8929760(7)
Epoch of the ascending node, Tasc (MJD)	58754.6813852(11)	58780.47407404(18)	–	59258.1366884(2)
$e \sin \omega$, ϵ_1 (10^{-5})	-1.85(12)	-0.130(10)	–	-0.024(18)
$e \cos \omega$, ϵ_2 (10^{-5})	1.29(12)	0.280(13)	–	0.133(12)
<i>Fixed Parameters</i>				
Solar System Ephemeris	DE438	DE438	DE438	DE438
Reference epoch for α , δ , and ν (MJD)	58907.554993	58809.870892	58781.000000	59492.667393
<i>Derived Parameters</i>				
Galactic longitude, l ($^\circ$)	47.494	50.126	47.131	95.152
Galactic latitude, b ($^\circ$)	-12.201	-14.765	-19.786	-58.988
DM-derived distance (YMW16 model), d (kpc)	3.78	2.09	4.54	0.96
Spin-down luminosity, \dot{E} (10^{33} erg s^{-1})	1.791(8)	3.25(2)	1.750(7)	2.47(3)
Surface magnetic field, B_{surf} (10^8 G)	3.169(7)	1.719(5)	7.562(15)	1.107(8)
Characteristic age, τ_c (Gyr)	7.49(3)	10.26(6)	3.177(13)	18.3(2)
Inferred eccentricity, e (10^{-5})	2.25(12)	0.308(12)	–	0.135(12)
Mass function, f (10^{-3}) M_\odot	0.4359286(8)	3.5469558(5)	–	5.4682203(14)
Minimum companion mass, $m_{c,min}$ (M_\odot)	0.099	0.209	–	0.245
Median companion mass, $m_{c,med}$ (M_\odot)	0.115	0.245	–	0.288
Longitude of the fiducial plane, ϕ_0 ($^\circ$)	113(1)	–	2(1)	–
Reference position angle ψ_0 ($^\circ$)	-80(2)	–	55(2)	–
Magnetic inclination angle, α ($^\circ$)	95(2)	–	124(11)	–
Viewing angle, ζ ($^\circ$)	118(2)	–	144(9)	–

given by [Phinney \(1992\)](#). This suggests that this system likely formed through the same evolution track as the other MSP binaries ([Phinney 1992](#); [Tauris & Savonije 1999](#)). However, this pulsar is also slightly unusual in having a spin period of 25.07 ms and an unusually small mass function; the latter is either caused by a small inclination or an unusually small companion mass.

In summary, our results and discussions have shown the following:

(1) We present the timing results of 12 newly discovered pulsars from CRAFTS survey. These pulsars were followed at FAST and Arecibo at L-band. We report the phase-connected timing ephemeris, polarization pulse profiles, and Faraday rotation measurements of these new MSPs. These pulsars are all MSPs, including eleven MSP - He WD systems and one isolated pulsar.

(2) We discuss the distribution of M_c and e in our newly discovered pulsars compared with the known MSP - He WD binary systems. PSR J1912–0952, PSR J0203–0150, PSR J0925+6103 and PSR J2001+0701 are four systems with eccentricity consistent with the prediction of [Phinney 1992](#) but with M_c lightly less than the prediction [Tauris & Savonije \(1999\)](#). This could be simply due to their systems having a low orbital inclination. The other seven

binaries discussed in this paper have eccentricities and companion masses that are consistent with the prediction of [Phinney 1992](#) and [Tauris & Savonije \(1999\)](#).

(3) As shown in the top panel of Fig 5, there exist a special out-lier group to the Phinney Orbit period and eccentricity relation – the so-called eccentric MSPs, which fall in an ‘orbit period gap’ ([Tauris 1996](#); [Freire & Tauris 2014](#); [Hui et al. 2018](#); [Han & Li 2021](#); [Lorimer et al. 2021](#)). The existence of this group indicates an alternative binary evolution channel that might have caused their unusually high orbital eccentricity. In our sample, PSR J1912–0952 is a low-eccentric MSP - He WD system ($e = 4.9 \times 10^{-5}$, $P_b \sim 29.49d$) that resides well in the ‘orbit period gap’. But its eccentricity and P_b follows closely the prediction given in [Phinney 1992](#). This system supports that at least some systems in this ‘orbit period gap’ are formed through the same channel as the other MSP binaries ([Martinez et al. 2019](#)).

(4) As shown in Fig. 2, PSR J1811–0624, PSR J1824–0621, and PSR J1908+0128 are three systems that have no data sets at the superior conjunction means we can’t measure Shapiro delay with the current data presented in this work. PSR J0203-0150, PSR J2355+0051, PSR J1813–0402, PSR J1929+0131, and PSR J2015+0755 are

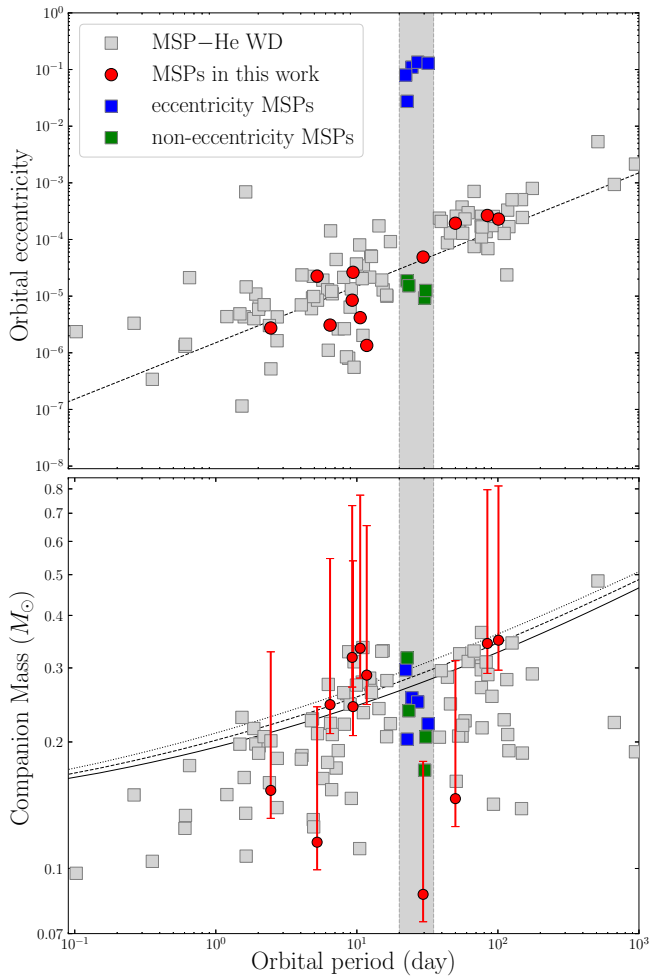


Figure 5. The MSP (spin periods shorter than 30 ms) with light white dwarf (WD) companions from the PSRCAT (version 1.6.5) (Manchester et al. 2005). MSP-WD systems are shown with grey squares. Eccentric systems in orbital period P_b ranging from 20 to 35 days are marked with blue squares and non-eccentric systems in this range are marked with green squares. The red filled dots are the binaries presented in this work. The orbital period P_b range where extra-eccentric MSP binary are often found, from 20 to 35 days is marked using shaded vertical bar. Top panel: The P_b and eccentricity e correlation for MSP with light WD companion systems. The dashed black line shows the theoretical relation of orbital period and eccentricity given in Phinney 1992. Bottom panel: The P_b and companion mass M_c correlation for binary pulsars with light WD companion systems. The dash and solid lines are numerical calculation from Tauris & Savonije 1999 for MSP - He WD systems. Median M_c estimates are given from their mass functions assuming an orbital inclination $i = 60^\circ$ and $M_{psr} = 1.4M_\odot$. The error bars are the minimum ($i = 90^\circ$) and 90 per cent probability ($i = 25.8^\circ$) M_c estimates.

five systems with few observations at the superior conjunction. In the current data sets, the Shapiro delay gives the limitation of $i < 75^\circ$. The other four PSR J1913–0952, PSR J2001+0701, and PSR J0825+6103 are binary systems with the timing residuals larger than the relativistic signal. The current timing precision limited the Shapiro delay measurements in these systems.

(5) Finally, we estimate that the flux density of these pulsars are greater than 0.1 mJy at 1.25 GHz. 11 of 12 MSPs have the timing rms smaller than 20 μ s (except PSR J1912–0952). We expect these 11 MSPs are the potential candidates for inclusion in PTAs and could

make a contribution to the PTA experiment from regular timing observations (Verbiest et al. 2016; Perera et al. 2019).

ACKNOWLEDGEMENTS

We thank the anonymous referee and Tasha Gautam for careful review and insightful comments that significantly improved the manuscript. This work made use of the data from FAST and Arecibo. FAST is a Chinese national mega-science facility, operated by National Astronomical Observatories, Chinese Academy of Sciences. The Arecibo Observatory was a facility of the National Science Foundation operated under cooperative agreement (#AST-1744119) by the University of Central Florida in alliance with Universidad Ana G. Méndez (UAGM) and Yang Enterprises (YEI), Inc. This work is supported by the National SKA Program of China No. 2020SKA0120200, the National Nature Science Foundation grant No. 12041303, 12041304, 11873067, U2031117, 11903049, 11703047, 11773041, U2031119, 12173052, 12103013, 12103069, 11903049, the National Key R&D Program of China No. 2017YFA0402600, the CAS-MPG LEGACY project, the Foundation of Science and Technology of Guizhou Province Nos. (2016)4008, (2017)5726-37,(2021)023, the Foundation of Guizhou Provincial Education Department (No.KY(2020)003,KY(2021)303), Guizhou Provincial Science and Technology Foundation (Nos. ZK[[2022]304). L. Zhang is funded by ACAMAR Postdoctoral Fellowship. PW was supported by the Youth Innovation Promotion Association CAS (id. 2021055) and the CAS Project for Young Scientists in Basic Research (grant YSBR-006). P. Wang and J. M. Yao were supported by Cultivation Project for FAST Scientific Payoff and Research Achievement of CAMS-CAS.

DATA AVAILABILITY

Origin raw data are published by the FAST data center and can be accessed through them. For other intermediate-process data, please contact the author (miaocc@nao.cas.cn).

REFERENCES

- Antoniadis J., et al., 2013, *Science*, **340**, 448
 Antoniadis J., Kaplan D. L., Stovall K., Freire P. C. C., Deneva J. S., Koester D., Jenet F., Martinez J. G., 2016, *ApJ*, **830**, 36
 Archibald A. M., et al., 2018, *Nature*, **559**, 73
 Barr E. D., et al., 2013, *MNRAS*, **435**, 2234
 Barr E. D., Freire P. C. C., Kramer M., Champion D. J., Berezina M., Bassa C. G., Lyne A. G., Stappers B. W., 2017, *MNRAS*, **465**, 1711
 Cameron A. D., et al., 2018, *MNRAS*, **475**, L57
 Cameron A. D., et al., 2020, *MNRAS*, **495**, 3515
 Camilo F., et al., 2015, *ApJ*, **810**, 85
 Cordes J. M., et al., 2006, *ApJ*, **637**, 446
 Cruces M., et al., 2021, *MNRAS*, **508**, 300
 Demorest P. B., Pennucci T., Ransom S. M., Roberts M. S. E., Hessels J. W. T., 2010, *Nature*, **467**, 1081
 Deneva J. S., Stovall K., McLaughlin M. A., Bates S. D., Freire P. C. C., Martinez J. G., Jenet F., Bagchi M., 2013, *ApJ*, **775**, 51
 Everett J. E., Weisberg J. M., 2001, *ApJ*, **553**, 341
 Fonseca E., et al., 2021, *ApJ*, **915**, L12
 Freire P. C. C., Ridolfi A., 2018, *MNRAS*, **476**, 4794
 Freire P. C. C., Tauris T. M., 2014, *MNRAS*, **438**, L86
 Gaia Collaboration et al., 2018, *A&A*, **616**, A1
 Han Q., Li X.-D., 2021, *ApJ*, **909**, 161
 Han J. L., et al., 2021, *Research in Astronomy and Astrophysics*, **21**, 107

- Hewish A., Bell S. J., Pilkington J. D. H., Scott P. F., Collins R. A., 1968, *Nature*, **217**, 709
- Hobbs G. B., Edwards R. T., Manchester R. N., 2006, *MNRAS*, **369**, 655
- Hobbs G., et al., 2010, *Classical and Quantum Gravity*, **27**, 084013
- Hotan A. W., van Straten W., Manchester R. N., 2004, *PASA*, **21**, 302
- Hui C. Y., Wu K., Han Q., Kong A. K. H., Tam P. H. T., 2018, *ApJ*, **864**, 30
- Jiang P., et al., 2020, *Research in Astronomy and Astrophysics*, **20**, 064
- Keith M. J., et al., 2010, *MNRAS*, **409**, 619
- Knispel B., et al., 2015, *ApJ*, **806**, 140
- Kramer M., Backer D., Cordes J., Lazio T., Stappers B., Johnston S., 2004, *New Astronomy Reviews*, **48**, 993
- Kramer M., et al., 2021, *Physical Review X*, **11**, 041050
- Lange C., Camilo F., Wex N., Kramer M., Backer D. C., Lyne A. G., Doroshenko O., 2001, *MNRAS*, **326**, 274
- Lewandowski W., Wolszczan A., Feiler G., Konacki M., Sołtysiński T., 2004, *ApJ*, **600**, 905
- Li D., et al., 2018, *IEEE Microwave Magazine*, **19**, 112
- Lorimer D. R., Kramer M., 2012, *Handbook of Pulsar Astronomy*
- Lorimer D. R., et al., 2021, *MNRAS*, **507**, 5303
- Manchester R. N., 2015, *IJMPD*, **24**, 1530018
- Manchester R. N., et al., 2001, *MNRAS*, **328**, 17
- Manchester R. N., Hobbs G. B., Teoh A., Hobbs M., 2005, *AJ*, **129**, 1993
- Martinez J. G., et al., 2019, *ApJ*, **881**, 166
- Miao X., Zhao J., Shao L., Wex N., Kramer M., Ma B.-Q., 2020, *ApJ*, **898**, 69
- Nan R., 2008, in Stepp L. M., Gilmozzi R., eds, *Society of Photo-Optical Instrumentation Engineers (SPIE) Conference Series Vol. 7012, Ground-based and Airborne Telescopes II*. p. 70121E, doi:10.1117/12.791288
- Nan R., et al., 2011, *International Journal of Modern Physics D*, **20**, 989
- Nice D., et al., 2015, *Tempo: Pulsar timing data analysis (ascl:1509.002)*
- Niu C.-H., et al., 2021, *ApJ*, **909**, L8
- Octau F., Cognard I., Guillemot L., Tauris T. M., Freire P. C. C., Desvignes G., Theureau G., 2018, *A&A*, **612**, A78
- Özel F., Freire P., 2016, *ARA&A*, **54**, 401
- Parent E., et al., 2019, *ApJ*, **886**, 148
- Perera B. B. P., et al., 2019, *MNRAS*, **490**, 4666
- Phinney E. S., 1992, *Philosophical Transactions of the Royal Society of London Series A*, **341**, 39
- Purcell C. R., Van Eck C. L., West J., Sun X. H., Gaensler B. M., 2020, *RM-Tools: Rotation measure (RM) synthesis and Stokes QU-fitting (ascl:2005.003)*
- Qian L., Yue Y., 2020, arXiv e-prints, p. arXiv:2012.08359
- Qian L., et al., 2019, *Science China Physics, Mechanics, and Astronomy*, **62**, 959508
- Radhakrishnan V., Cooke D. J., 1969, *Astrophys. Lett.*, **3**, 225
- Ransom S., 2011, *PRESTO: Pulsar Exploration and Search TOolkit (ascl:1107.017)*
- Sanidas S., et al., 2019, *A&A*, **626**, A104
- Sayer R. W., Nice D. J., Taylor J. H., 1997, *ApJ*, **474**, 426
- Serylak M., et al., 2022, arXiv e-prints, p. arXiv:2203.00607
- Shao L., Caballero R. N., Kramer M., Wex N., Champion D. J., Jessner A., 2013, *CQGra*, **30**, 165019
- Sotomayor-Beltran C., et al., 2013, *A&A*, **552**, A58
- Spiewak R., et al., 2020, *MNRAS*, **496**, 4836
- Stovall K., et al., 2014, *ApJ*, **791**, 67
- Stovall K., et al., 2018, *ApJ*, **854**, L22
- Stovall K., et al., 2019, *ApJ*, **870**, 74
- Tauris T. M., 1996, *A&A*, **315**, 453
- Tauris T. M., Savonije G. J., 1999, *A&A*, **350**, 928
- Taylor J. H., Weisberg J. M., 1989, *ApJ*, **345**, 434
- Verbiest J. P. W., et al., 2016, *MNRAS*, **458**, 1267
- Voisin G., Cognard I., Freire P. C. C., Wex N., Guillemot L., Desvignes G., Kramer M., Theureau G., 2020, *A&A*, **638**, A24
- Wang S., et al., 2021a, *Research in Astronomy and Astrophysics*, **21**, 251
- Wang P., et al., 2021b, *Science China Physics, Mechanics, and Astronomy*, **64**, 129562
- Wang S. Q., et al., 2021c, *ApJ*, **922**, L13
- Yao J. M., Manchester R. N., Wang N., 2017, *ApJ*, **835**, 29
- You S., et al., 2021, arXiv e-prints, p. arXiv:2110.12749
- Yu Q.-Y., et al., 2020, *Research in Astronomy and Astrophysics*, **20**, 091
- Zhang L., et al., 2019, *ApJ*, **877**, 55
- Zhu W. W., et al., 2019a, *MNRAS*, **482**, 3249
- Zhu W. W., et al., 2019b, *ApJ*, **881**, 165
- Zhu W. W., et al., 2020, *ApJ*, **895**, L6
- van Straten W., Bailes M., 2011, *PASA*, **28**, 1

This paper has been typeset from a $\text{\TeX}/\text{\LaTeX}$ file prepared by the author.